Dynamic Feedback in Wave-Mediated Surface Haptics: A Modular Platform

Dustin Goetz*
Department of Mechanical Engineering
University of California, Santa Barbara
Santa Barbara, CA 93106 USA
dgoetz@ucsb.edu

Gregory Reardon*
Media Art and Technology Program
University of California, Santa Barbara
Santa Barbara, CA 93106 USA
reardon@ucsb.edu

Max Linnander
Department of Mechanical Engineering
University of California, Santa Barbara
Santa Barbara, CA 93106 USA
maxlinnander@ucsb.edu

Yon Visell
Biological Engineering Program
University of California, Santa Barbara
Santa Barbara, CA 93106 USA
yonvisell@ucsb.edu

Abstract—**Emerging surface haptic technologies exploit wave physics to create software-programmable two-dimensional haptic displays. However, designing such systems is challenging due to the complex dependence of wave propagation on the system's hardware arrangement, materials, and boundary conditions. We present a modular system for exploring design opportunities for wave-mediated haptic feedback via elastic surfaces. The system integrates an array of repositionable, custom electromagnetic actuators that excite shear waves which propagate in a reconfigurable elastic medium. We use optical vibrometry imaging to capture data that fully encode the transmission of waves in this system. We present methods that leverage the linearity of wave transport and the acquired data to efficiently implement and evaluate a variety of hardware configurations and software methods for displaying dynamic, spatially-resolved two-dimensional haptic feedback. These techniques can allow researchers to rapidly investigate methods for engineering software-programmable surface haptic displays based on wave excitation.**

Index Terms—**Surface Haptics, Wave Focusing, Haptic Device, Haptic Rendering**

I. INTRODUCTION

A longstanding goal in haptics has been to realize displays that can furnish dynamic, high-fidelity haptic feedback in perceptually rich spatial detail. This objective has led several groups to investigate devices that provide spatiotemporally-resolved haptic feedback via distributed arrays of micromechanical actuators [1]–[4]. However, to match the tremendous spatial and temporal acuity of the human haptic system, the required number of physical degrees of freedom, and thus actuators, far exceed what would be practical, in cost or complexity, within the state-of-the-art [5].

Emerging underactuated haptic feedback techniques are able to furnish greater spatial resolution, with fewer actuators, than is possible in conventional haptic displays. One such technique involves wave-mediated surface haptic devices, which are characterized by their ability to deliver high-resolution haptic feedback through the propagation of surface waves on a flat or curved surface [6]–[8]. Using these methods, dynamic haptic feedback can be delivered to computationally-specified spatial locations, surpassing the limitations of traditional, fully-actuated haptic displays [9]–[11].

However, designing such wave-mediated surface haptic devices presents a complex challenge that encompasses both hardware design and rendering methods. The properties of the generated waves are dependent on the material properties, geometry, and boundary conditions of the transport medium, while the number, location, and bandwidth of the actuated elements determine the system's forced solution set. These interdependent factors greatly encumber progress in research, demanding experimental approaches that often involve time-consuming fabrication, simulation, and vibrometry measurement steps.

To overcome these limitations and accelerate research on wave-mediated haptics, we introduce a modular platform for exploring design opportunities for wave-mediated haptic feedback via elastic surfaces. This approach circumvents burdensome experimental demands, allowing for rapid investigation of various design options and rendering techniques. Our platform integrates a reconfigurable driving system and interchangeable elastic media and support structures. Our methodology is enabled by our use of high-resolution optical vibrometry to capture data encoding the physics of wave transmission via the ensemble of Green's functions. By leveraging these data, and exploiting the linearity of the system, we can accurately assess the spatiotemporal attributes of haptic feedback produced in various hardware configurations and by different rendering algorithms without any requirement for further measurements. We show, in experiments, that this methodology can produce an expressive range of spatially- and temporally-resolved haptic feedback, highlighting the promise of this approach.
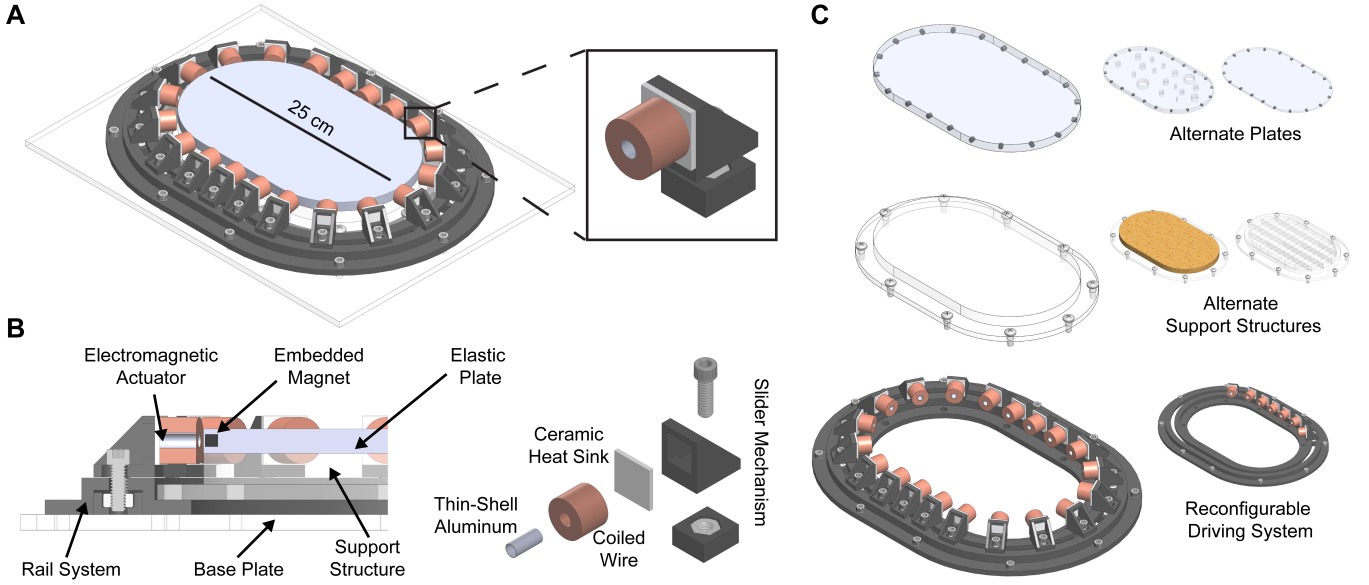
Fig. 1. A) Our device consists of an elastic plate surrounded by 20 electromagnetic actuators. The actuators are driven to produce software-specified mechanical vibrations on the plate surface which can be easily felt by users. B) The actuators are constructed from electromagnetic coils mounted on thin-shell aluminum bobbins and ceramic heat sinks. These actuators drive magnets that are embedded in the plate, producing spatially distributed vibrations on the plate's surface. A support structure and 3D-printed rail system are used to finely position the plate and actuators. C) Our device is easy to reconfigure, allowing us to rapidly assess the attributes of haptic feedback produced in various hardware configurations. Because of the non-contact actuation design, the plates and support structures can be easily exchanged with alternates. With our custom rail system, individual actuators can quickly be removed or repositioned.

II. MODULAR SURFACE-HAPTIC PLATFORM

Our platform encompasses a reconfigurable hardware device and techniques for using data obtained from one-time vibrometry characterizations in data-driven experiments. The methods described below make it possible to rapidly and empirically assess the performance of the device, or feedback characteristics, in a variety of configurations.

A. Hardware Design and Fabrication

Our device consists of an elastomer surface haptic plate that is driven by an array of 20 circumferentially-distributed electromagnetic actuators (Fig. 1A). The plate thickness is $1\,\mathrm{inch}$, with a Bunimovich stadium cross-section (parameters: $a = 10\,\mathrm{cm}$, $r = 7.5\,\mathrm{cm}$) – dimensions that allow an entire hand to contact the surface. Each actuator is a custom-wound electromagnetic coil (diameter: $2\,\mathrm{cm}$, thickness: $1.5\,\mathrm{cm}$) that produces magnetic fields that exert forces on adjacent magnets (diameter: $0.5\,\mathrm{cm}$, thickness: $0.5\,\mathrm{cm}$) embedded in the elastomer plate. The elastic plate sits atop an acrylic slab support structure (thickness: $1.3\,\mathrm{cm}$) and the actuators can be repositioned around the perimeter of the plate via a custom rail system (Fig. 1B). Because the electromagnetic coils are decoupled from the elastomer, it is possible to easily exchange the elastomer plate or support structure for others of various materials or geometries (Fig. 1C). These hardware components – the elastic plate and support structure – can be selected or designed to alter the transport physics of mechanical waves excited by the system [12]–[14], thus making it possible to

explore opportunities or performance characteristics of different configurations.

To fabricate the elastic plate, synthetic gelatin (Humimic Gelatin #2, Humimic, USA; mass density: $923.5\,\mathrm{kg/m^3}$, Young's modulus: $260\,\mathrm{kPa}$) was cast using a custom polycarbonate mold. Magnets (Cylo158, SuperMagnetMan, USA) were embedded using positioning holes stamped in the elastomer via a 3D-printed pillar structure, after which additional synthetic gelatin was added, and distributed via heat application. This process embedded the magnets approximately $1\,\mathrm{mm}$ from the edge of the plate.

The electromagnetic coil design was obtained via analyses that ensured it could produce forces as large as $0.25\,\mathrm{N}$ acting on the magnets. The coil's electrical properties (resistance: $14\,\Omega$, inductance: $5\,\mathrm{mH}$) are compatible with commodity audio hardware. To fabricate each electromagnetic coil, 30-AWG magnet wire was wound (950 turns) about a thin-shell aluminum bobbin. For heat dissipation, each coil was mounted to a ceramic heat sink using thermally conductive adhesive (8329TFF, MG Chemicals, Canada).

The coils were concentrically aligned with the magnets using a 3D-printed rail system. The 20 actuator signals delivered to the coils were furnished via computer, output via a 24-channel digital-to-analog-converter (24Ao, MOTU, USA), and amplified by two 12-channel audio amplifiers (MA1240a, Dayton Audio, USA; PT12050CH, Pyle, USA). This configuration permitted audio-rate control of all actuator outputs.

We fabricated two different support structures via laser engraving: a fully-supporting solid acrylic plate (Fig. 2B) and a
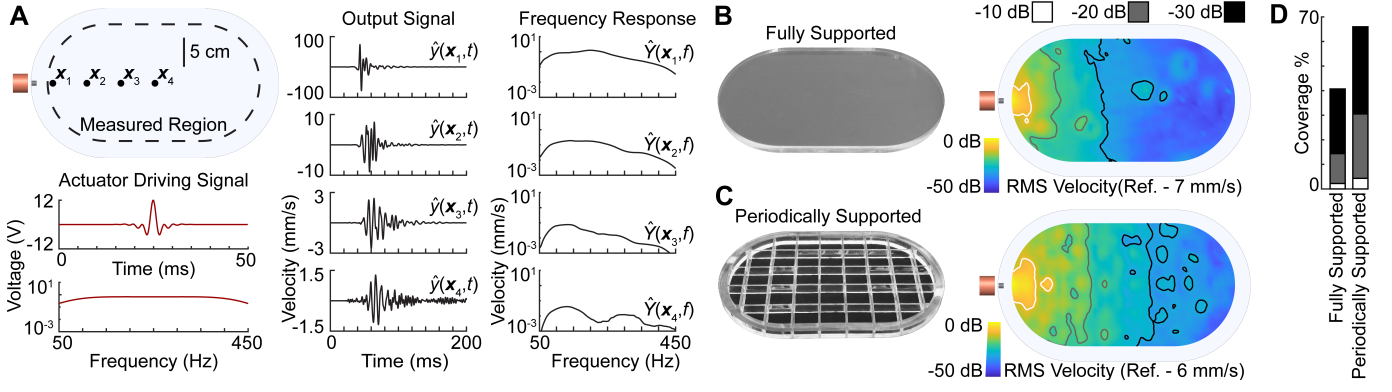
Fig. 2. A) Experimental results of the system response to a bandlimited pulse (50−450 Hz) emitted from a single actuator at multiple locations on the plate's surface (computed via convolution with measured Green's functions). The time-varying output velocity and frequency response on the surface of the elastic plate display effects of both dispersion and dissipation. B) Actuators excite confined regions near to themselves with a median −20 dB dropoff of 5.3 cm (RMS surface velocity and −10 dB, −20 dB, and −30 dB contours shown). C) Energy transmission in the plate was enhanced when using a periodic support structure due to the free boundary conditions within each unit cell. D) The periodic support structure enhanced transmission in the plate by nearly a factor of 2 (total plate surface area [as a percentage of total surface area] covered by the −10, −20, and −30 dB contours for each support structure shown).

periodically-supporting acrylic grid (2.5 cm grid cell; Fig. 2C). The cross-section of the support matched that of the elastic plate. The support was adhered to a fixed base plate and mounted on a pneumatically isolated optical table. Results reported in the paper were obtained using the solid acrylic plate support, except where otherwise noted.

B. Vibrometry Measurements

We performed optical vibrometry measurements to capture Green's functions encoding wave transport in the plate. We leverage the measurements, and exploit the linearity of the system, in efficient data-driven experiments that are performed by convolving specified (arbitrary) actuator signals with measured Green's functions to accurately deduce the resulting oscillations in the medium.

The physics of vibration transmission can be described by a linear wave equation $Ly(\boldsymbol{x}, t) = \sum_i f_i(\boldsymbol{x}, t)$, where L is a viscoelastic wave partial differential operator. $f_i(\boldsymbol{x}, t) = u_i(t)\delta(\boldsymbol{x} - \boldsymbol{x}_i)$ is the force exerted by the ith actuator at location $\boldsymbol{x}_i$, $u_i(t)$ is the driving signal, and $y(\boldsymbol{x}, t)$ is the oscillation velocity across the surface of the medium. While elastic wave oscillations are vectorial, those produced here are treated as scalar, with the device actuated and measured along one axis.

The Green's functions $g(\boldsymbol{x} - \boldsymbol{x}_i, t)$ describe the oscillation response at $\boldsymbol{x}$ that is produced by a delta function impulse at the respective actuator location, $\boldsymbol{x}_i$. Our vibrometry measurements yield measured Green's functions $\hat{g}_i(\boldsymbol{x}, t) \approx g(\boldsymbol{x} - \boldsymbol{x}_i, t)$. Using these data, the wave oscillations that would result from applying arbitrary driving signals $u_i(t)$ can be obtained via convolution:

$$\hat{y}(\boldsymbol{x}, t) = \sum_{i=1}^{N} \hat{g}_i(\boldsymbol{x}, t) * u_i(t), \tag{1}$$

We captured the ensemble of Green's functions $\hat{g}_i(\boldsymbol{x}, t)$ for all i, $\boldsymbol{x}$, and t by measuring wave oscillations excited by driving each of the 20 actuators with 3-second linear sinusoidal sweep

test signals (20−500 Hz, 3 repetitions). The excited oscillations were captured via a scanning laser Doppler vibrometer (Type 8330 SLDV, Ometron, UK, data sample rate $f_s = 10$ kHz, 14 bits) at a grid of locations in a region spanning most of the elastomer surface (Fig. 2A, top left panel). The spatial sample period δ was selected to satisfy a spatial Nyquist criterion, as empirically determined from pilot measurements. We applied this procedure in order to measure Green's functions for the two device configurations: fully supported condition (sample period $\delta = 4$ mm; Fig. 2B) and periodically supported condition ($\delta = 5$ mm; Fig. 2C). The measurements yielded approximately 55 hours of recorded data. We computed the empirical Green's functions from these data using sine sweep deconvolution [15], which were subsequently employed for the convolutions in our data-driven experiments.

In related work by the authors, we verified that wave oscillations $\hat{y}(\boldsymbol{x}, t)$ obtained from such data-driven experiments closely match those that can be obtained from independent vibrometry measurements [11]. This technique is also extremely efficient, since the data-driven experiments require only seconds to perform, while independent vibrometry measurements require hours of experiment time to collect. Thus, we used this data-driven method of experimentation for the remainder of this contribution.

C. Wave Transmission Characteristics

We characterized wave transmission in the plate by driving each actuator with a bandlimited impulse $u_i(t)$ (impulse bandwidth: 50−450 Hz; Fig. 2A bottom left panel). Wave transmission was highly dispersive (Fig. 2A, middle panel), with a group velocity of approximately 4.8 m/s, estimated via envelope tracking of the bandlimited impulse. Damping was frequency-dependent. High frequencies (> 200 Hz) rapidly attenuated with distance (Fig. 2A, middle panel), consistent with theory [12], [16]–[18]. Due to damping and geometric attenuation, excited oscillation amplitudes were largest at
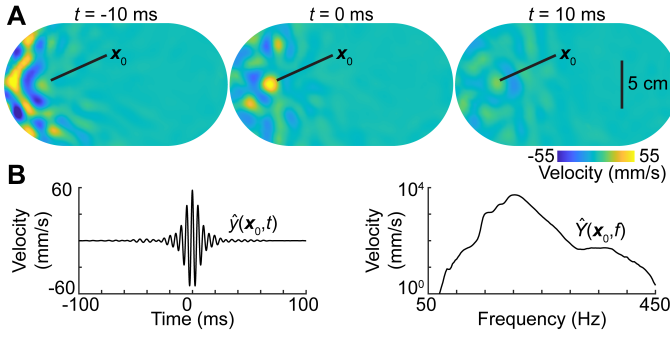
Fig. 3. A) Experimental results of focused wave field rendering on a fully supported plate with 20 independently-driven actuators (surface velocity at three different time points shown). Time-reversal focusing causes energy to converge onto the specified focus location $\boldsymbol{x}_0$ at a specified time (focus time set to $t = 0$ for convenience). Waves converge onto the location over a short time and rapidly decay. B) Time-varying velocity and frequency response at the focus location $\boldsymbol{x}_0$ reflects the response characteristics of our system.

locations near to the driven actuator (Fig. 2B). Waves propagated with distance-dependent attenuation of approximately $-3.8\,\mathrm{dB/cm}$, averaged across all actuators. These losses were reduced in the periodically supported condition (Fig. 2C). Consequently, the surface areas encompassed by the $-10, -20$, and $-30\,\mathrm{dB}$ contours were $1.97, 1.85$, and 1.38 times larger in the periodically supported condition.

III. EXPLORING RENDERING METHODS AND CONFIGURATIONS

The modularity of our design and the efficiency of our experimental method made it possible to rapidly obtain results for different algorithms for rendering spatially-resolved 2D haptic feedback and different hardware configurations. We informally explored dozens of alternatives, with selected results presented in this section.

A. Localized Feedback via Time-Reversal Focusing

We explored the ability of the platform to supply localized haptic feedback in different configurations using time-reversal focusing of wave oscillations [19]. This approach has also been exploited in prior wave-mediated surface haptic research [6], [8], [9], [11].

In time-reversal focusing, waves are focused to a location, $\boldsymbol{x}_0$, by driving actuators using the time-reversed Green's function evaluated at the focal location

$$u_i(t) = \hat{g}_i(\boldsymbol{x}_0, T - t) * s(t) \qquad (2)$$

Here, $s(t)$ is the signal content to be delivered at $\boldsymbol{x}_0$ beginning at time T. In the special case that $s(t)$ is a delta impulse, $\delta(t)$, oscillations at the focal location $\boldsymbol{x}_0$ approximate a bandlimited Dirac delta function with frequency content that is determined by the Green's function from the actuators to the focus location (Fig. 3).

We quantitatively assessed the focusing capabilities of our system in four different configurations. Three of these configurations investigated focusing with different numbers of

actuators, acting individually or in interleaved groups controlled with common driving signals. The first, second, and third rows of Fig. 4, respectively, present results obtained using all actuators (row 1), using a unilateral array of 7 actuators (row 2), and using 20 actuators controlled in 4 interleaved groups, with each group controlled by a common driving signal (row 3). A fourth configuration (Fig. 4A, fourth row) used 20 independently-controlled actuators with a periodically supported plate (row 4). We set $s(t) = \delta(t)$ in the experiments. Focus quality was assessed for all possible focal locations on the surface (Fig. 4C, D, respectively), by computing the focus diameter and focus energy ratio at the focus time $t = T$ at each focus location. The focus diameter was computed as the spatial full width at half maximum of the focused signal. The focus energy ratio was computed as the ratio of the mean RMS energy density within the focus diameter to the mean RMS energy density outside of it.

Due to viscoelastic damping, the unilateral display condition (row 2) yielded lower focal quality in the more distant half of the display. Relative to the case in which all 20 actuators were driven independently (row 1), focal diameters for the unilateral display (row 2) were 17% larger on the more distant side, and the focus energy ratio was $9\,\mathrm{dB}$ lower. Further analyses revealed that the anisotropic distribution of spatial frequency content yielded prominent secondary focal sidelobes. In the grouped actuator condition (row 3), focal quality was on par with the 20 independent actuator condition (row 1). Focus quality was best in the periodically supported plate configuration (row 4), yielding an average focal diameter of $7.16\,\mathrm{mm}$, which is on the order of vibrotactile spatial acuity of the human fingertip [20]. The focal diameters in this configuration were, on average, 18% smaller when compared to the 20-actuator condition with the fully supported plate (row 1; see Supplementary Video). Further, due to the reduced attenuation, focus quality near the center of the plate was best in the periodically supported condition (row 4), and the variance of the focal diameter decreased by half compared with the fully supported condition (row 1; variance $0.46\,\mathrm{mm}^2$ versus $1.02\,\mathrm{mm}^2$).

B. Rendering Distributed Spatiotemporal Feedback

We also explored methods for rendering distributed spatiotemporally patterned feedback that can be felt over extended regions of the surface. We demonstrate two of many possible rendering methods that can be produced by synthesizing simple or complex driving signals – one based on simple harmonic scanning wavelet synthesis and another based on stochastic wavelet synthesis.

1) Scanning Wavelet Synthesis: The first distributed feedback method employed a simple wavelet-based approach, in which the center frequency of wavelets emitted from each actuator increased from $150\,\mathrm{Hz}$ to $300\,\mathrm{Hz}$ along the major axis of the device (Fig. 5A1). The wavelet's amplitude envelope was a trapezoidal window shape of fixed duration. Wavelet emission occurred in a delayed temporal sequence along a specified direction, yielding a constant-velocity apparent motion-like scanning pattern (Fig. 5A2) that varied linearly in frequency
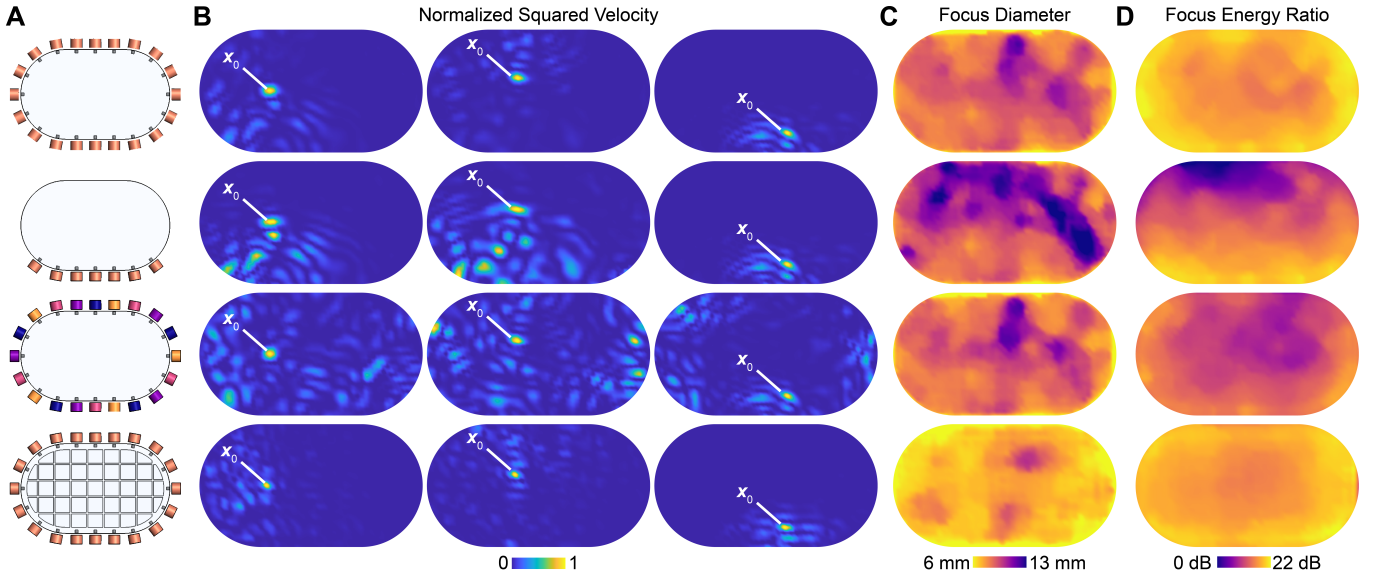
Fig. 4. A) Different hardware configurations were assessed via time-reversal focusing experiments (first row: fully supported plate, 20 actuators; second row: fully supported plate, unilateral array of 7 actuators; third row: fully supported plate, 20 actuators controlled in 4 interleaved groups [denoted by color] driven by common signals; fourth row: periodically supported plate, 20 actuators). B) Normalized squared velocity, $y(\mathbf{x}, T)^2 / \max_{\mathbf{x}}[y(\mathbf{x}, T)^2]$, of experimental wave fields for each of the different configurations at 3 different exemplar focusing locations at focus time T. C) Focus diameter (defined in Section IIIA) computed at focus time T when focusing to each calibrated location on the display. D) Focus energy ratio (defined in Section IIIA) computed at focus time T when focusing to each calibrated location on the display.

content across the display (Fig. 5A3). We adjusted the wavelet amplitudes to ensure approximately constant intensity at all frequencies. We designed and selected three patterns (see Supplementary Video) that were evaluated in a brief perceptual study (Sec. IV). The velocity of the scanning pattern, the direction of scanning, and the wavelet duration varied among the three patterns.

2) Stochastic Wavelet Synthesis: The second algorithm was based on stochastic spatiotemporal wavelet synthesis. Wavelets emitted from each actuator were determined by stochastic sampling of the frequency, start time, amplitude, duration, and actuator location (Fig. 5B1). This synthesis algorithm produced disordered wave oscillation patterns (Fig. 5B2). The frequency content varied heterogeneously across the display surface (Fig. 5B3). We used this method to design and select three additional feedback patterns (see Supplementary Video) for use in the perceptual study (Sec. IV). The wavelet patterns were specified by changing the probability distribution of the parameters for each of the three patterns.

IV. PERCEPTION OF HAPTIC FEEDBACK

We conducted two brief perceptual experiments to illustrate how users perceived feedback supplied by the system. One experiment was based on the spatial localization of focused oscillations (Sec. III-A). The second assessed the perception of distributed feedback rendered using the two wavelet techniques (Sec. III-B1, III-B2) in a free description task. In both experiments, the participant's volar hand surface lightly contacted the plate. Participants wore circumaural headphones that played pink noise to mask auditory cues. The protocol was approved

by the human subjects review board at the authors' institution. All 10 participants completed both tasks (5 male, 5 female; maximum hand size: $21\,\mathrm{cm}$; median age: 25.5). Each gave their written, informed consent.

The localization experiment used a five-alternative choice task. Participants felt stimuli focused at one of five hand locations: wrist, pinky, thumb, fingertips, or center (Fig. 6A) and reported the location at which they felt the feedback. Localized feedback was generated using time-reversal focusing (Sec. III-A). The excitation signal $s(t)$ was a train of short, noise bursts ($50\,\mathrm{ms}$ noise burst, $150\,\mathrm{ms}$ pause, 10 bursts). Participants responded verbally and could request stimuli to be replayed, but rarely did so. To facilitate familiarization with the device and procedure, participants felt all 5 stimuli before the experiment began and were not provided any feedback or informed of the focus locations. Stimuli were presented in randomized order. Each location was presented 10 times. Responses were correct in 96.7% of trials (483 out of 500; Fig. 6B). Response accuracy was lowest for the "center" location but still averaged 89% at this location. The modest decline may be due to the fact that waves focused to that location would have first traversed surface locations below other hand areas. The high response accuracies preclude meaningful statistical analysis but also underline the ease with which participants localized the feedback.

The second experiment evaluated the perception of distributed spatiotemporal feedback, using a free description task. Participants were not provided any information about the stimuli, other than general details about the procedure. Participants felt a different stimulus on each trial. They then supplied
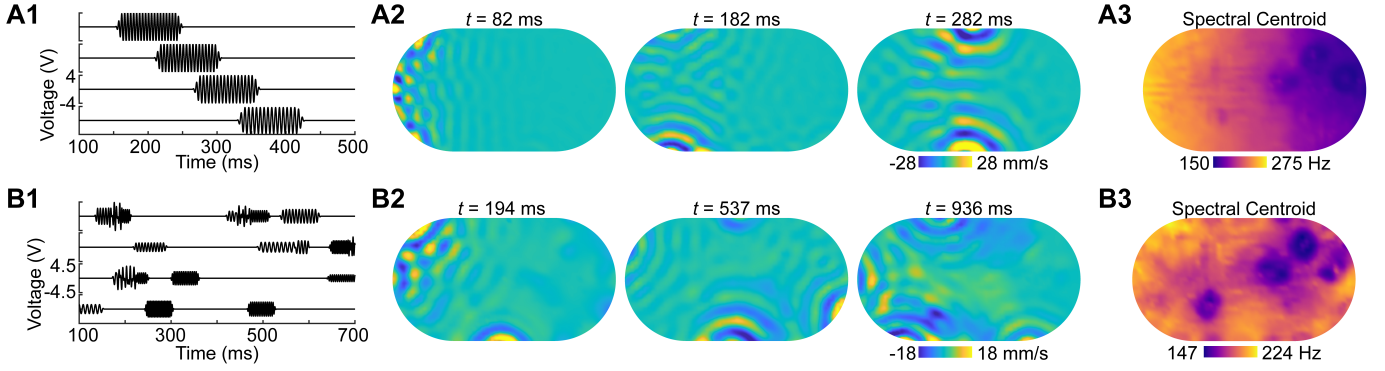
Fig. 5. A) Experimental wave field results for scanning wavelet synthesis. Synthesis occurs via short wavelet signals offset in time and emitted from each actuator (A1). This driving pattern produced mechanical waves on the plate which scanned across the display (A2) and yielded frequency content (A3; spectral centroid at each calibrated location shown) which varied linearly across the device. B) Experimental wave field results for stochastic wavelet synthesis. Synthesis occurs via wavelet signals with stochastically determined parameters (B1). Mechanical energy is distributed throughout (B2) in an uncontrolled manner and frequency content (B3; spectral centroid at each calibrated location shown) across the display was heterogeneous.
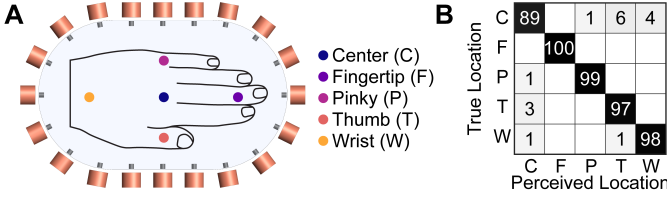

Fig. 6. A) Perceptual localization experiment. Time-reversal focusing delivered feedback to surface locations below five hand locations. B) Confusion matrix (all experimental trials shown) for the localization experiment illustrates the high localization accuracy at all hand locations (96.7% total accuracy; chance: 20%).

written descriptions of the stimulus, before proceeding to the next trial. Participants felt 3 designed scanning wavelet stimuli and 3 designed stochastic wavelet stimuli in the experiment (see Supplementary Video). The order of presentation of the stimuli was randomized. The patterns were repeated as many times as the participant preferred. Participants described the scanning patterns using a variety of terms including "scanning," "sweeping," or "petting." (Participants' characterizations of these stimuli as "scanning" informed the name we applied to these stimuli in this paper). The stochastic patterns were also described using a variety of terms, including "rain," "swirly," or "discrete." Unique descriptor sets were supplied for different stimuli in each category by nearly all participants. One of the scanning patterns was described by all participants using terms that referred to a "heartbeat" or "pulse." One participant described the surface as feeling "alive" in this case. One of the stochastic patterns was often described using terms such as "spiky," "sharp," and "electric."

V. CONCLUSION

We presented a modular platform for exploring the design and rendering of wave-mediated surface haptic feedback. Our reconfigurable platform and efficient data-driven experimental methodology allowed us to rapidly explore and evaluate different rendering techniques and hardware configurations. Our findings demonstrated that modifications to boundary conditions improved energy transmission in a highly damped medium and enhanced our system's ability to deliver localized haptic feedback. Our experiments also showed that our rendering algorithms can provide perceptually evocative, spatially- and temporally-resolved haptic feedback.

Our results proved remarkably robust to loading the surface via light touch contact with the hand at, and near to, the focus locations. The effects of interfacial contact with the skin on wave transport are complex and are not theoretically or experimentally characterized here. Further research would be merited.

Wave-mediated surface haptic displays offer exciting unexplored possibilities. These displays provide spatially-resolved dynamic feedback, similar to spatial audio or video displays. The methodology reported here could accelerate advancements in this area of research. It can enable the rapid investigation of techniques for focusing localized haptic feedback, rendering distributed haptic scenes, or generating source motion effects. These methods can also be used to determine hardware configurations or designs with different geometries or materials that promote wave transport, and the design of novel haptic feedback methods. In short, our data-driven experimental methodology, and the modular hardware design approach we demonstrate, provide valuable tools for advancing research in wave-mediated surface haptics.

REFERENCES

[1] Juan José Zárate and Herbert Shea. Using pot-magnets to enable stable and scalable electromagnetic tactile displays. *IEEE Transactions on Haptics*, 10(1):106–112, 2016.
[2] Yasushi Ikei, Kazufumi Wakamatsu, and Shuichi Fukuda. Vibratory tactile display of image-based textures. *IEEE Computer Graphics and Applications*, 17(6):53–61, 1997.

[3] Carter Compton Collins. Tactile television-mechanical and electrical image projection. *IEEE Transactions on Man-Machine Systems*, 11(1):65–71, 1970.

[4] Olivier Bau, Uros Petrevski, and Wendy Mackay. Bubblewrap: a textile-based electromagnetic haptic display. In *CHI'09 Extended Abstracts on Human Factors in Computing Systems*, pages 3607–3612. 2009.

[5] Shantonu Biswas and Yon Visell. Emerging material technologies for haptics. *Advanced Materials Technologies*, 4(4):1900042, 2019.

[6] Charles Hudin, Jose Lozada, and Vincent Hayward. Localized tactile feedback on a transparent surface through time-reversal wave focusing. *IEEE Transactions on Haptics*, 8(2):188–198, 2015.

[7] Ravish Mehra, Christoph Hohnerlein, David Perek, Elia Gatti, Riccardo DeSalvo, and Sean Keller. Hapticwave: directional surface vibrations using wave-field synthesis. In *ACM SIGGRAPH 2016 Emerging Technologies*, pages 1–2. 2016.

[8] Gregory Reardon, Nikolas Kastor, Yitian Shao, and Yon Visell. Elastowave: Localized tactile feedback in a soft haptic interface via focused elastic waves. In *2020 IEEE Haptics Symposium (HAPTICS)*, pages 7–14. IEEE, 2020.

[9] Lucie Pantera and Charles Hudin. Multitouch vibrotactile feedback on a tactile screen by the inverse filter technique: vibration amplitude and spatial resolution. *IEEE Transactions on Haptics*, 13(3):493–503, 2020.

[10] Jung-Han Woo and Jeong-Guon Ih. Vibration rendering on a thin plate with actuator array at the periphery. *Journal of Sound and Vibration*, 349:150–162, 2015.

[11] Gregory Reardon, Dustin Goetz, Max Linnander, and Yon Visell. Rendering dynamic source motion in surface haptics via wave focusing. *IEEE Transactions on Haptics*, 2023.

[12] Bradley E Treeby and Ben T Cox. Modeling power law absorption and dispersion for acoustic propagation using the fractional laplacian. *The Journal of the Acoustical Society of America*, 127(5):2741–2748, 2010.

[13] Ayoub Ben Dhiab and Charles Hudin. Confinement of vibrotactile stimuli in narrow plates. In *2019 IEEE World Haptics Conference (WHC)*, pages 431–436. IEEE, 2019.

[14] Thomas Daunizeau, David Gueorguiev, Sinan Haliyo, and Vincent Hayward. Phononic crystals applied to localised surface haptics. *IEEE Transactions on Haptics*, 14(3):668–674, 2021.

[15] Piotr Majdak, Peter Balazs, and Bernhard Laback. Multiple exponential sweep method for fast measurement of head-related transfer functions. *Journal of the Audio Engineering Society*, 55(7/8):623–637, 2007.

[16] Jan Achenbach. *Wave propagation in elastic solids*. Elsevier, 2012.

[17] Sverre Holm. *Waves with power-law attenuation*. Springer, 2019.

[18] Chunfang Yuan, Suping Peng, Zhongjie Zhang, and Zhenkuan Liu. Seismic wave propagating in kelvin-voigt homogeneous visco-elastic media. *Science in China Series D*, 49(2):147–153, 2006.

[19] Mathias Fink. Time reversal of ultrasonic fields. i. basic principles. *IEEE Transactions on Ultrasonics, Ferroelectrics, and Frequency Control*, 39(5):555–566, 1992.

[20] C.A. Perez, C.A. Holzmann, and H.E. Jaeschke. Two-point vibrotactile discrimination related to parameters of pulse burst stimulus. *Medical and Biological Engineering and Computing*, 38:74–79, 2000.